ELSEVIER

Ceramics International 27 (2001) 571–576

CERAMICS INTERNATIONAL

www.elsevier.com/locate/ceramint

Reactions between SiC and sintering aids in Si_3N_4/SiC nanocomposites and their consequences

Rongcan Zhou *, Zhongchao Feng, Yong Liang, Feng Zheng, Quangang Xian

Institute of Metal Research, Chinese Academy of Sciences, Shenyang 110016, China

Received 28 August 2000; received in revised form 30 October 2000; accepted 28 November 2000

Abstract

Si_3N_4/SiC nanocomposites were fabricated by hot-pressing mixtures of submicron α- Si_3N_4, SiC nanopowders with sintering aids. XRD, TEM and SEM were used to study the effects of SiC additions on sintering behavior and microstructure of Si_3N_4; EDAX was employed to investigate the composition of interfaces. The results showed that nano-SiC addition led to loss and compositional modification of intergranular phases and limited the densification and phase transformation of Si_3N_4. Reactions between sintering aids and nano-SiC are thermodynamically calculated and the temperature and N_2 pressure dependence of the reactions are also theoretically analyzed. Influences of these reactions on the effects of SiC additions are discussed.

Keywords: A. Sintering; B. Nanocomposites; D. SiC; D. Si_3N_4; Reactions

1. Introduction

Silicon nitride-based ceramics have attracted much attention for several decades due to their potential application in various fields [1]. Nanometric SiC particles have been found to be effective additions in improving the mechanical properties of Si_3N_4 [2–4]. A large number of studies have been made in the Si_3N_4/SiC nanocomposite system. These works revealed that both densification and the α→βphase transformation of Si_3N_4 during sintering were inhibited by nano-SiC. Despite the inconsistent results of fracture toughness other mechanical properties, especially high temperature properties, were significantly improved by nanometric SiC dispersions. However, the cause of the above effects was not quite clear, and the study of the mechanism is of great importance. It is well known that the amount, composition and distribution of grain boundary phases have a great influence upon the sintering behavior, microstructure and properties of Si_3N_4. Reactions between SiC and sintering aids may take place and then contribute to above results. However, only reactions between SiO_2 and SiC have been discussed thermodynamically until now [3,4], with little data on reactions between SiC, Al_2O_3 and Y_2O_3, often used as sintering aids in Si_3N_4. The purpose of the present work was to investigate the reactions between nanometric SiC addition and the sintering aids of Si_3N_4 and their consequences

2. Experimental procedures

2.1. Preparation of materials

Si_3N_4 powders (0.9 μm, $\alpha \geqslant 95\%$, Shanghai Material Institute, China,) and SiC nanopowders (20 nm, β-SiC, Institute of Metal Research) were used as raw materials. Al_2O_3 (30 nm, 99.95%, Institute of Solid Physics) and Y_2O_3 (3–4 μm, 99.99%, Hunan Rare Earth Institute) were selected as sintering aids.

Mixtures of Si_3N_4 powder, various volume fractions of nano-SiC (0, 5, 20 vol.%) and 6 wt.%Y_2O_3 + 2 wt.% Al_2O_3 were dispersed in a 100 W ultrasonic bath for 10 min then ball-milled for 24 h using ethanol as a dispersant in a nylon vessel. The slurries were vacuum dried and 100 g mixed powders were hot pressed in a BN-doped graphite die (85 mm in diameter) at 1680–1750°C for 45 min in a N_2 atmosphere with a pressure of 30 MPa.

* Corresponding author.
E-mail address: rezhou@imr.ac.cn (R. Zhou).

0272-8842/01/$20.00
PII: S0272-8842(01)00003-7

2.2. Characterization

The densities of the sintered bodies were measured by the Archimedes method. The crystalline phases of the hot-pressed materials were determined by X-ray diffraction analysis (XRD) on a D/max-RA diffractometer with CuK_α radiation ($\lambda = 0.1541$ nm) on the surfaces perpendicular to the hot-pressing direction; the relative contents of α-Si_3N_4 in the samples were calculated according to Suzuki et al. [5]. The microstructure was observed using a scanning electron microscope (SEM, Philips-XL30 FEG) on polished and NaOH-etched samples. A TEM specimen of Si_3N_4/5 vol.% SiC was prepared and analyzed by a analytical transmission electron microscope (TEM, Philips EM420) equipped with an energy-dispersive X-ray spectrometry unit (EDAX 9100), used to determine the relative element contents of Al, Y, Si within Si_3N_4 grains and at various interfaces.

3. Results

The relative densities of sintered bodies decreased with increasing SiC content, as shown in Fig. 1. This indicated that the nano SiC addition hindered the densification of Si_3N_4. Fig. 2 shows the X-ray diffraction patterns of the three samples. Owing to the low sintering temperature and short dwell time, α-Si_3N_4 was identified in all the three samples. The α phase contents of the sintered bodies are plotted in Fig. 1. The inhibition of α-$Si_3N_4 \rightarrow \beta$-$Si_3N_4$ phase transformation by the SiC addition, reported by other authors [6], was also observed in the present study; SiC was remained as the β phase. In addition to the main phases, some small peaks of intergranular phases occurred (Fig. 2). In monolithic Si_3N_4, the peaks of $Y_{20}N_4Si_{12}O_{48}$, α-$Y_2Si_2O_7$ and $Y_5N(SiO_4)_3$ were relatively strong, in Si_3N_4/5 vol.%SiC, moderate peaks of α-$Y_2Si_2O_7$ were observed, while in Si_3N_4/20 vol.% SiC, only traces of α-$Y_2Si_2O_7$ were identified; these indicated that the amounts of intergranular crystalline phases decreased with increasing amounts of SiC.

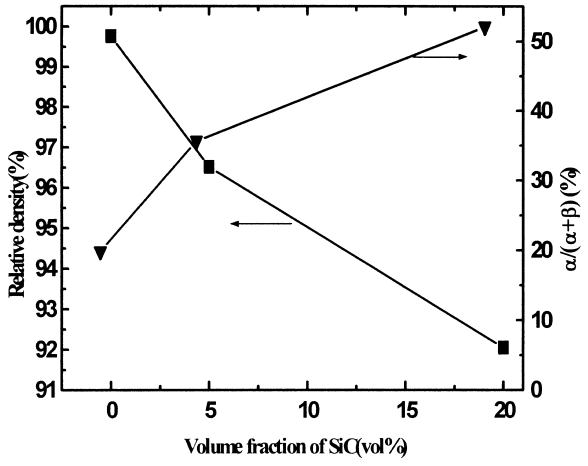

Fig. 1. Relative densities and α-Si_3N_4 fraction of the sintered bodies.

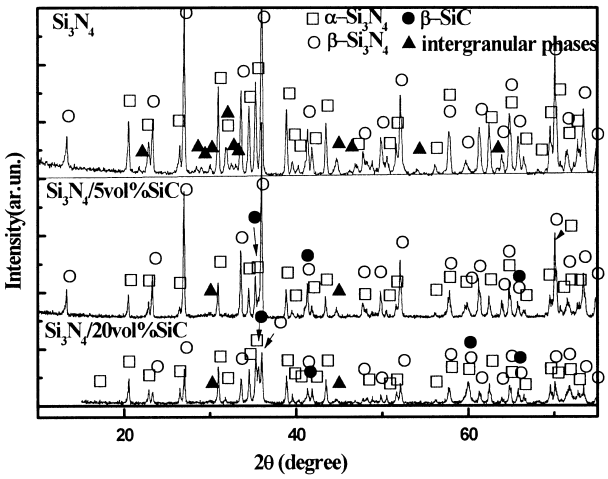

Fig. 2. X-ray diffraction patterns of sintered bodies.

Fig. 3 shows the SEM micrographs of the etched samples. With increasing SiC, the average size of Si_3N_4 grains became smaller and the growth of Si_3N_4 grains was restrained by the SiC nano particles.

Fig. 4 shows the TEM images of Si_3N_4/5 vol.% SiC. Some SiC particles were dispersed within Si_3N_4 grains and at grain boundaries (Fig. 4a); some were aggregated at grain boundaries (Fig. 4b). In the EDAX analyses, representative plots (See Fig. 5) were analyzed. These plots included three types: spots at the Si_3N_4 grain boundary which had different distances from a cluster of SiC particles (A, B and C in Fig. 5); spots at different Si_3N_4/SiC phase boundaries (D, E and F in Fig. 5) and a spot in a Si_3N_4 grain (G). According to the EDAX results, the relative contents of Si, Al and Y at selected spots are list in Table 1. At the Si_3N_4 grain boundaries (points A, B, C in Fig. 5), the amounts of Y and Al elements (Table 1) were proportional to the distance between the measured spots and nearby SiC particles. The Y and Al contents at the Si_3N_4/SiC interfaces were also related to their positions. For a SiC particulate within a Si_3N_4 grain (F in Fig. 5), considering the dilution because a part of SiC, in which Y and Al are absent, was probably included in the analysis, the Y and Al contents of Si_3N_4/SiC

Table 1
EDAX results of interfaces

Interface	Si_3N_4/Si_3N_4			Si_3N_4/SiC			Si_3N_4 grain
Plot	A	B	C	D	E	F	G
Si (wt.%)	76.3	68.7	61.0	85.0	88.3	89.4	88.7
Al (wt.%)	9.1	10.7	13.8	10.2	9.7	8.8	9.5
Y (wt.%)	14.6	20.6	25.2	4.2	2.0	1.9	2.8

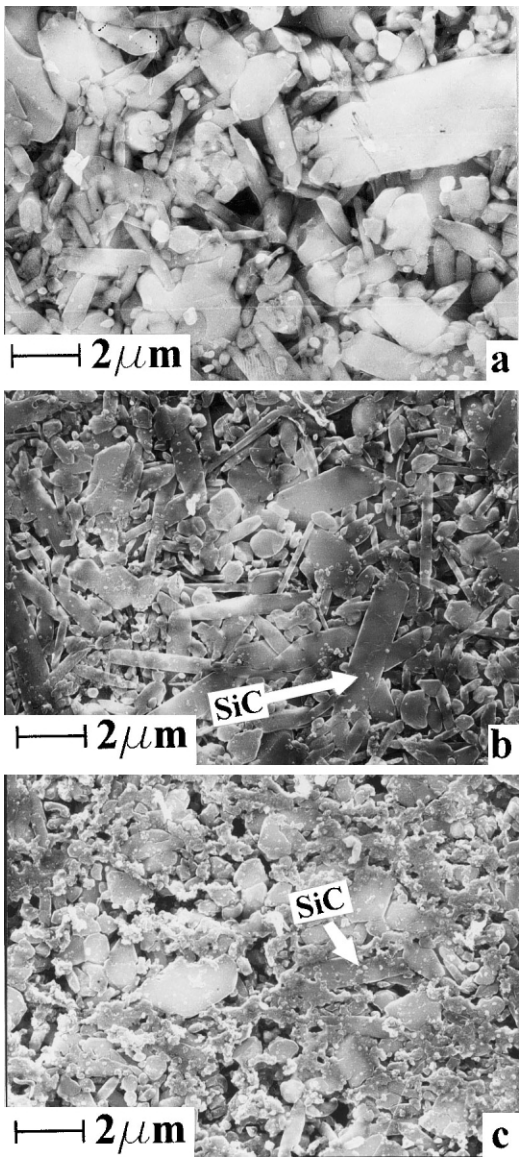

Fig. 3. SEM images of (a) Si_3N_4, (b) Si_3N_4/5 vol.% SiC and (c) Si_3N_4/20 vol.% SiC.

interface were close to those of Si_3N_4 grains (point G in Fig. 5), it is suggested that the interface was clean and SiC was directly bonded to Si_3N_4; this was quite consistent with results by other authors [7]. For a SiC particle located at the Si_3N_4 grain boundary, Y and Al contents of Si_3N_4/SiC interfaces (points D and E in Fig. 5) were higher than those of a point at the Si_3N_4/SiC interface within a Si_3N_4 grain (F), but lower than the spot at the Si_3N_4/ Si_3N_4 interface and far from SiC (Point A in Fig. 5), especially at point E, where the SiC particle was partly surrounded by a Si_3N_4 grain. The dilution resulting from the amount by SiC in the analysis was estimated and referred to that between F and G. Although the EDAX is only semi-quantitative, the results could indicate that the SiC particles decreased the nearby Y and Al contents.

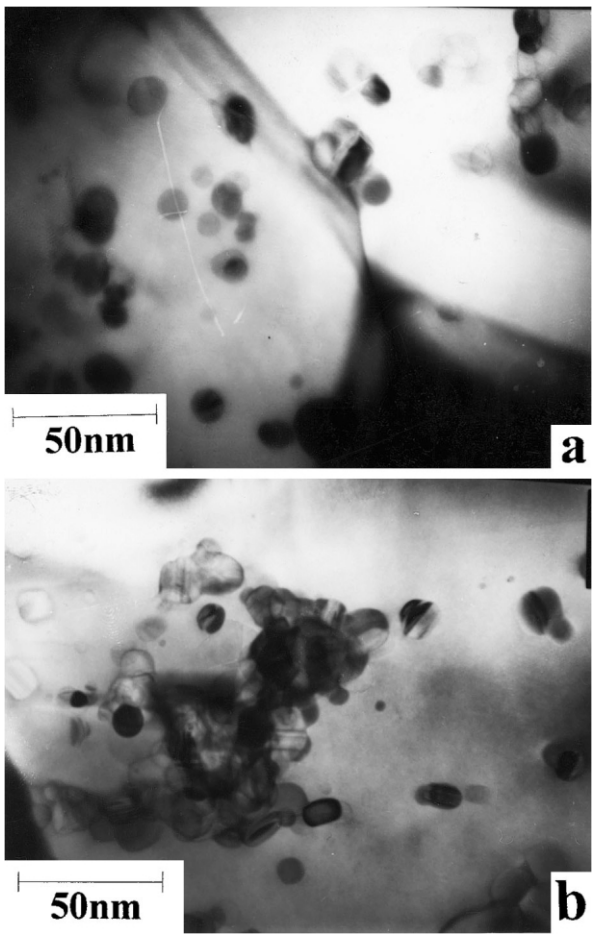

Fig. 4. TEM micrographs of Si_3N_4/5 vol.% SiC. (a) SiC dispersed within Si_3N_4 grain and at grain boundary (b) aggregates of SiC particles.

4. Discussion

The addition of nano-SiC led to a decrease of the diffraction intensities of intergranular phases as shown by XRD, this indicated that SiC decreased the amounts of intergranular phases. For the same sintering condition and low cooling rate, this difference revealed that materials had different amounts of liquids at high temperatures. However, additions of sintering aids to the three samples were the same; a reasonable explanation was the nano-SiC addition resulted in loss of the liquid phase. The EDAX results showed that the plots near the SiC particles had a lower Y, Al contents, which also demonstrated that the SiC addition led to the loss of sintering aids. The samples were restricted in the graphite dies, so the only way in which the loss of sintering aids could occur was the reaction between nano-SiC and sintering aids and formation of volatile gases.

To simplify the discussion of the interactions between SiC and sintering aids (including SiO_2 at the powder surfaces), it is assumed that the sintering aids reacted with nano-SiC in their original states and individually, although they actually formed a melt.

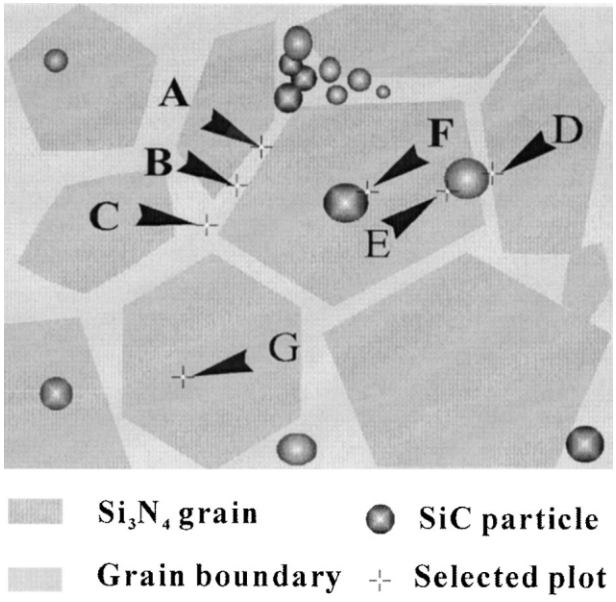

Fig. 5. Schematic diagram of selected plots in EDAX analyses.

The following reactions between SiC and SiO_2 have been reported previously [3].

$$SiC(s,\ \beta) + 2SiO_2(l\ org) \rightarrow 3SiO\ (g) + CO(g) \quad (1)$$

$$2SiC(s,\ \beta) + SiO_2\ (lorg) + 2N_2(g) \rightarrow Si_3N_4\ (s) + 2CO(g) \quad (2)$$

The reactions of SiC with Al_2O_3 and Y_2O_3 have not been thermodynamically calculated. The following reactions may result in loss of sintering aids.

$$SiC(s,\beta) + 2Al_2O_3(s) \rightarrow 4AlO(g) + SiO(g) + CO(g)\Delta G_T = 3567546.4 - 1105.54312T + RT\ln\left(P_{CO}\cdot P_{SIO}\cdot P_{AlO}^4\right) \quad (3)$$

$$SiC(s,\beta) + Al_2O_3(s) \rightarrow SiO(g) + Al_2O(g) + CO(g)\Delta G_T = 1403140 - 565.297T + RT\ln(P_{SIO}\cdot PAl_2O\cdot P_{CO}) \quad (4)$$

$$6SiC(s,\beta) + 3Al_2O_3(s) + 4N_2(g) \rightarrow 2Si_3N_4(s) + 3Al_2O(g) + 6CO(g)\Delta G_T = 2910450 - 1076.25T + RT\ln\left(\frac{P_{Al_2O}^3\cdot P_{CO}^6}{P_{N_2}^4}\right) \quad (5)$$

$$SiC(s,\beta) + 2Y_2O_3(s) \rightarrow 4YO(g) + SiO(g) + CO(g)\Delta G_T = 3520725.877 - 1358.107T + 47.778T + 49.778T\ln T + RT\ln\left(P_{YO}^4\cdot P_{SIO}\cdot P_{CO}\right) \quad (6)$$

$$SiC(s,\beta) + Y_2O_3(s) \rightarrow Y_2O(g) + SiO(g) + CO(g)\Delta G_T = 176954.2 - 734.104T + 22.116T\ln T + RT\ln(P_{Y2O}\cdot P_{SIO}\cdot P_{CO}) \quad (7)$$

$$6SiC(s,\beta) + 3Y_2O_3(s) + 4N_2(g) \rightarrow 3Y_2O(g) + 2Si_3N_4(s) + 6CO(g)\Delta G_T = 3985654.712 - 1541.3875T + 65.392T\ln T + RT\ln\left(\frac{PY_{2O}^3P_{CO}^6}{P_{N_2}^4}\right) \quad (8)$$

"(s)" denotes solid phase, "(l)"denotes liquid phase, "(g)" denotes gas phase, ΔG_T denotes the Gibbs free energy change in J of the reaction at temperature T (1300–2100 K). Thermochemical data were taken from the literature [8–10]. Due to the insufficiency of data, ΔS_{298}^o, the entropy at 298 K of Y_2O was estimated according to the formula put forward by Kubaschewski et al. [10].

Assuming the reactions are enough to reach equilibrium and the gas phases can exchange freely in the furnace space (about 1 m^3 in the present study), when equilibrium has been reached, the calculated sintering aids consumption (ΔW_{cal}) at different sintering temperature and under different nitrogen pressure is shown in Fig. 6. Temperature has a great influence on the reactions of all the aids; N_2 pressure has no effect on reactions (1), (3), (4), (6) and (7) but influences the others. A cooperative effect of temperature and N_2 pressure is observed in reactions 5 and 8; the consumption of aids increases greatly when temperature and N_2 pressure were simultaneously raised. As a synthetic effect, the consumption of all sintering aids increases with the increasing of sintering temperature and N_2 pressure. As the results show, the most possible mechanisms of volatilization of sintering aids are reactions (1), (2), (4), (5) and (8). SiO_2 is susceptible to vaporization while Al_2O_3 has moderate stability and Y_2O_3 is the most stable; there is an order of magnitude difference between them, for example, the calculated consumption of SiO_2, Al_2O_3 and Y_2O_3 by reactions (1), (2), (4), (5) and (8) at 2000 K and under 1 atm N_2 pressure was respectively 167.5, 119.9, 2.63, 3.92 and 0.043 g.

With the given assumption, SiO_2 and Al_2O_3 in the samples would have been exhausted. In real sintering conditions, reaction would not proceed to such an extent due to sluggish kinetics and the physical containment provided by the graphite dies. At another extreme, assuming the atmosphere was restricted exactly to within the graphite dies (the capacity was about 0.0005 m^3), the consumption of the sintering aids would be about 0.0005 ΔW_{cal}, which could be neglected except for SiO_2. Due to the exchange of the atmosphere to some extent across the dies in real sintering condition, the real consumption was $\alpha\Delta W_{cal}$ ($0.0005 < \alpha < 1$), it was in proportion to the effective diffusing-room for the atmosphere. Because loss of Si can be compensated by dissolution of Si_3N_4,

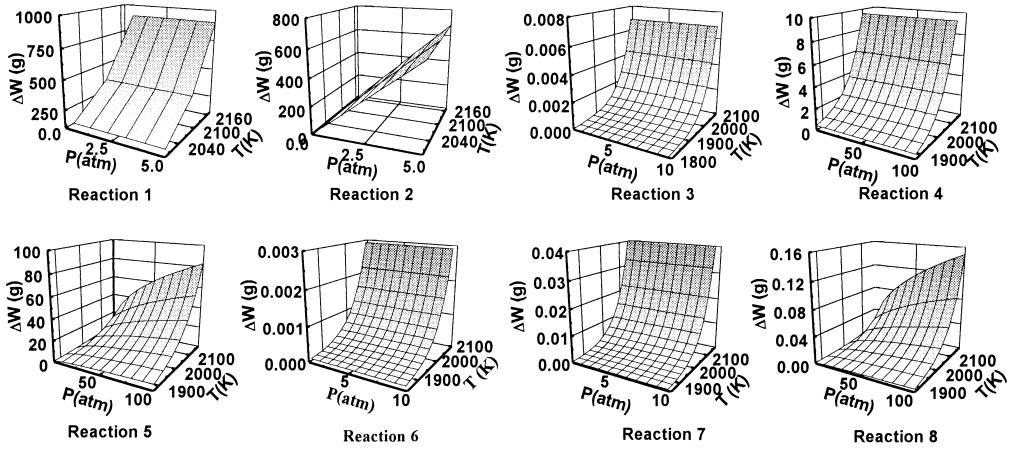

Fig. 6. Temperature (T) and nitrogen pressure (P) dependence of consumption(ΔW) of sintering aids.

only the decrease and gradient distribution of Y and Al element content around SiC was revealed in the EDAX results.

The disproportional volatilization of different aids would tend to decrease contents of SiO_2 and Al_2O_3 in the grain boundary phases. According to the phase diagram of the Y_2O_3–Al_2O_3–SiO_2 system [11] (Fig. 7), for the common sintering aids compositions, 6 wt.% Y_2O_3 + 2 wt.% Al_2O_3 or 8 wt.% Y_2O_3 and usual oxygen content (<2.0 wt.%) in starting Si_3N_4 powders, decrease of SiO_2 and Al_2O_3 contents will increase softening temperature and thus influence other properties of the melt phase, which is presented as glass.

The amount and composition of the liquid phase plays an important role in the sintering of Si_3N_4 [1]; the SiC addition resulted in loss of aids and modified the composition of intergranular phases, thus inhibiting densification, the $\alpha \rightarrow \beta$ phase transformation and the growth of β-Si_3N_4 grains. To sinter the Si_3N_4/SiC nanocomposites to full density, it is necessary to add more sintering aids to compensate for vaporization, especially of SiO_2 and Al_2O_3, and limit these loss through processing conditions such as using the crucible and powder bed technique, regulating sintering temperature and N_2 pressure, etc. On the other hand, the consumption of sintering aids will lead to the improvement of high temperature properties [2].

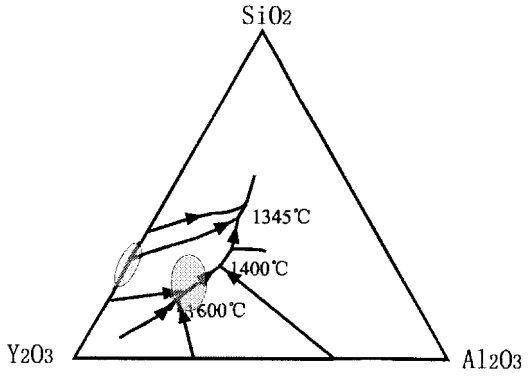

Fig. 7. Phase diagram of the Y_2O_3–Al_2O_3–SiO_2 system.

5. Conclusions

This study has drawn the following conclusions:

1. The nano-SiC addition lead to the loss and composition modification of intergranular phases.
2. The sintering aids are thermodynamically unstable in presence of SiC at high temperatures; SiO_2 is most susceptible to vaporization, Al_2O_3 is more stable than SiO_2 but more active than Y_2O_3. The reactions between nano-SiC and sintering aids caused the loss of the aids; the consumption amounts were greatly increased with increasing temperature and nitrogen pressure.
3. The quantitative and compositional changes due to SiC addition is the reason for the inhibition of densification, $\alpha \rightarrow \beta$ phase transformation and refine the microstructure of Si_3N_4.

Acknowledgements

The authors gratefully acknowledge the National Key Laboratory of Novel Ceramics and Fine Processing, China for funding to the research.

References

[1] G. Ziegler, J. Heinrech, G. Wötting, Relationships between processing, microstructure and properties of dense and reaction-bonded silicon nitride, J. Mater. Sci. 229 (1987) 3041–3086.
[2] M. Sternitzke, Review: structural ceramic nanocomposites, J. Eur. Ceram. Soc. 17 (1997) 1061–1082.
[3] M. Herrmann, C. Schuber, A. Rendtel, H. Hübner, Silicon nitride/silicon carbide nanocomposite materials: I. Fabrication

and mechanical properties at room temperature, J. Am. Ceram. Soc. 81 (5) (1998) 1095–1108.
[4] A. Rendtel, H. Hübner, M. Herrmann, C. Schuber, Silicon nitride/silicon carbide nanocomposite materials: II. Hot strength, creep, and oxidation resistance, J. Am. Ceram. Soc. 81 (5) (1998) 1109–1120.
[5] K. Suzuki, Y. Kanno, A conventional determination of α-phase fraction in Si_3N_4, J. Ceram. Soc. Jpn 92 (2) (1984) 101–102.
[6] S. Sato, M.C. Chu, J.H. Kim, Y. Kobayashi, K. Ando, Influence of SiC particle size on microstructure and mechanical properties of Si_3N_4/SiC composite ceramics, J. Ceram. Soc. Jpn 103 (7) (1995) 676–679.
[7] K. Niihara, K. Izaki, A. Nakahira, The Si_3N_4–SiC nanocomposites with high strength at elevated temperatures, J. Jpn Soc. Powder and Powder Metall. 37 (2) (1990) 172–179.
[8] W.E. Acree, et al. (Eds.), CRC Handbook of Physical Chemistry, 70th Edition, CRC Press, 1989–1990.
[9] Y. Dalun, Practical Handbook of Thermodynamic Properties of Inorganic Substances, Metallurgy Press, Beijing, 1981 (in Chinese).
[10] O. Kubaschewski, C.B. Alcock, Metallurgical Thermochemistry, Metallurgy Press, Beijing, 1985 (Chinese translation, pp. 233).
[11] N.A. Toropov, V.P. Brazakovski, V.V. Lapin, N.N. Kurtseva, Phase Diagrams, Vol. 3, Nauka, Moscow, 1972.